**Atmospheric
Chemistry
and Physics**
Discussions

Open Access

Diurnal variations of aerosol optical properties in the North China Plain and their influences on the estimates of direct aerosol radiative forcing

Y. Kuang[1], C. S. Zhao[1], J. C. Tao[1], and N. Ma[1,2]

[1]Department of Atmospheric and Oceanic Sciences, School of Physics, Peking University, Beijing, China
[2]Leibniz Institute for Tropospheric research, Leipzig, Germany

Correspondence to: C. S. Zhao (zcs@pku.edu.cn)

ACPD

15, 339–369, 2015

Diurnal variations of aerosol optical properties and their radiative effects

Y. Kuang et al.

Title Page

Abstract	Introduction
Conclusions	References
Tables	Figures

Back | Close

Full Screen / Esc

Printer-friendly Version

Interactive Discussion

Abstract

In this paper, the diurnal variations of aerosol optical properties and their influences on the estimation of daily average direct aerosol radiative forcing (DARF) in the North China Plain (NCP) are investigated based on in-situ measurements from Haze in China
5   campaign. For ambient aerosol, the diurnal variations of single scattering albedo (SSA) and asymmetry factor (g) in the NCP are both evident, and far different from those of dry state aerosol. The relative humidity is the dominant factor which determines the diurnal pattern of SSA and g for ambient aerosol. Basing on the calculated SSA and g, several cases are designed to investigate the impacts of the diurnal changes of
10 aerosol optical properties on DARF. The results demonstrate that the diurnal changes of SSA and g in the NCP have significant influences on the estimation of DARF at the top of the atmosphere (TOA). If the full temporal coverage of aerosol optical depth (AOD), SSA and g are available, an accurate estimation of daily average DARF can be achieved by using the daily averages of AOD, SSA and g. However, due to the lack
15 of full temporal coverage datasets of SSA and g, their daily averages are usually not available. Basing on the results of designed cases, if the RH plays a dominant role in the diurnal variations of SSA and g, we suggest that using both SSA and g averaged over early morning and late afternoon as inputs for radiative transfer model to improve the accurate estimation of DARF. If the temporal samplings of SSA or g are too few to
20 adopt this method, either averaged over early morning or late afternoon of both SSA and g can be used to improve the estimation of DARF at TOA.

1   Introduction

The direct effect of atmospheric aerosol on the radiation budget of earth is commonly described by direct aerosol radiative forcing (DARF). DARF can be estimated from
25 global aerosol models directly (Myhre et al., 2013), observations (Bellouin et al., 2005, 2008), or a combination of these two methods (Su et al., 2013). Most observation-

340

based methods use satellite data of aerosol optical depth (AOD) in combination with aerosol optical properties retrieved from ground-based sunphotometers from Aerosol Robotic Network (AERONET) (Holben et al., 1998), where the single scattering albedo (SSA) and asymmetry factor (g) are usually held constant (Myhre, 2009; Bellouin et al.,
5   2013). However, variations of the aerosol optical properties, including AOD, SSA and g, significantly impacts on the estimates of daily average DARF, and thus the monthly and annually averaged DARF as well.

The spatial and temporal distributions of aerosol optical properties are sampled either from space or at the earth's surface. For instance, the Moderate Resolution Imag-
10   ing Spectroradiometer(MODIS) onboard Terra and Aqua pass over the equator in the morning and afternoon, respectively. Thus, temporal coverage of aerosol optical properties retrieved from satellites is limited for specific time periods. In addition, the widely used ground-based AERONET retrievals provide AOD at relatively higher temporal resolution, but the intensive optical properties (SSA and g) retrieved from AERONET
15   measurements are typically limited to shorter time periods in the morning and afternoon when the solar zenith angle (SZA) is quite large ($50° \leq SZA \leq 70°$) (Holben et al., 2006; Dubovik et al., 2000; Kassianov et al., 2013). The incomplete temporal samplings of aerosol optical properties may be incapable of faithfully reproducing the diurnal variation of aerosol optical properties, especially for SSA and g. Therefore, the aerosol op-
20   tical properties are usually assumed to be constants (Sena et al., 2013; Myhre, 2009) or with negligible variability through the day of interest (Remer and Kaufman, 2006). So far, significant diurnal changes of AOD have been frequently observed in many polluted regions around the world (Zhang et al., 2012; Mazzola et al., 2010; Smirnov et al., 2002), but diurnal changes of SSA and g for ambient aerosol are rarely investigated.
25   The diurnal variations of these optical properties have rarely been taken into account in the measurement-based estimates of DARF. Arola et al. (2013) exploited data from a large number of AERONET sites, and assessed the influence of diurnal AOD variability on the estimates of daily average DARF at the top of atmosphere (TOA). Their results demonstrated that, for individual sites, there can be significant biases in the

estimates of DARF due to the diurnal AOD variability. However, if averaged over all AERONET sites, the influence of diurnal changes of AOD on the daily averaged DARF is rather small, even for cases in which AOD is taken either from Terra or Aqua overpass time. But the diurnal changes of SSA and g were not considered, and seasonal aver-
ages were used in this research. Kassianov et al. (2013) also assessed the impacts of diurnal variations of aerosol optical properties on the estimates of daily averaged DARF. Their results demonstrated that even in the presence of strong diurnal changes of AOD, an accurate prediction of daily average DARF requires only daily averaged aerosol optical properties. Nevertheless, the diurnal variations of SSA and g were not
also considered in this research due to their small ranges.

With the rapid growth of population and economy in China, emissions of anthropogenic pollutants have increased dramatically in recent decades, and China is suffering very serious air pollutions. The high aerosol loading in the NCP is an important factor which affects regional climate change due to their potential radiative effects (Zhao
et al., 2006), an accurate estimation of DARF in this region are therefore important. The published results from Haze in China (HaChi) campaign demonstrated that many aerosol physical and chemical properties have significant diurnal variations (Ma et al., 2011; Liu et al., 2011; Ran et al., 2011; Xu et al., 2011), which are different from the results for other regions around the world. Some scientific questions regarding the diurnal
variation of aerosol optical properties in the NCP arose: (1) What are the characterizations of diurnal variations of aerosol optical properties in the NCP, such as SSA and g? (2) Does the diurnal variations of aerosol optical properties have significant impacts on the estimation of daily average DARF in the NCP?

In this paper, the diurnal variations of SSA and g at ambient and dry conditions is
presented at a regional background site in the NCP. The calculated SSA and g are used to investigate the influences of their diurnal variability on the estimates of daily average DARF at TOA and surface. This is the first time, in the NCP, that the diurnal cycles of SSA and g are both taken into account in the prediction of daily average DARF. This is particularly important for studying the direct aerosol effect in the NCP

where absorbing and scattering aerosols may contribute significantly to the climate change of earth system (Chung et al., 2005; Bond et al., 2013).

In Sect. 2, the site information and related instruments are introduced. Data and methods used in this research are described in Sect. 3. Section 4 presents the calculated diurnal variations of aerosol optical properties and their influences on the estimates of daily average DARF. Finally, conclusions are reached in Sect. 5.

2 Site description and instruments

In this study, we use the dataset from the HaChi project which is conducted jointly by Peking University, China and Leibniz-Institute for Tropospheric Research, Germany at Wuqing (39°23′ N, 117°01′ E). This observation campaign lasted for about one month from 12 July 2009 to 14 August 2009. Wuqing site is located at the northern part of the NCP, between two megacities, Beijing and Tianjin. The distance between Wuqing and downtown Beijing is about 80 km, and is about 30 km between Wuqing and downtown Tianjin. Wuqing site is mainly surrounded by farmland and residential areas. The emission sources nearby are similar to those in most parts of the northern NCP. Hence, as a regional background site, the observational results in Wuqing can, to a large extent, represent the background aerosol properties in the northern NCP.

The particle number size distribution (PNSD) ranging from 3 nm to 10 μm was observed jointly by an Aerodynamic Particle Sizer (APS, TSI Inc., Model 3321) and a Twin Differential Mobility Particle Sizer (TDMPS, Leibniz-Institute for Tropospheric Research (IfT), Germany; Birmili et al., 1999) with a temporal resolution of 10 min at relative humidity lower than 30 %. The absorption coefficient at 637 nm was measured using a Multi-angle Absorption Photometer (MAAP Model 5012, Thermo, Inc., Waltham, MA USA) with a temporal resolution of 1 min, and further transformed into black carbon (BC) mass concentrations with a constant mass absorption efficiency (MAE) of 6.6 m^2 g^{-1}. The growth factors of aerosols at relative humidity spanning 0 to 98 % are obtained from the observation of the High Humidity Tandem Differential Mobility Ana-

lyzer (HH-TDMA, Leibniz-Institute for Tropospheric Research (IfT), Germany; Hennig et al., 2005). The HH-TDMA measured the growth factor at four selected particle diameters (50, 100, 200 and 250 nm) and three relative humidity conditions (90, 95 and 98.5 %). For detailed information of the measurements, please refer to Ma et al. (2011) and Liu et al. (2011).

Furthermore, ambient relative humidity with one-minute temporal resolution was measured by an automatic weather station (AWS). Other observational data (e.g. scattering coefficient at wavelengths of 450, 550 and 700 nm) used to retrieve the mixing state of light absorbing aerosol are in another study (Ma et al., 2012).

3 Data and methods

3.1 Calculation of aerosol optical properties

The estimation of DARF requires some aerosol optical properties, such as AOD, SSA and g. In this study, the AOD data from AERONET measurements were used (Holben et al., 2006). SSA and g were calculated using the measurements from HaChi campaign, considering both the mixing state of light absorbing carbonaceous (LAC) aerosol and the hygroscopic growth.

Ma et al. (2012) proposed a new method to retrieve the mixing state of LAC. In this method, aerosol chemical components are separated into two classes based on their refractive indices: the LAC and the less absorbing components. And dry-state aerosols are classified into two assumed types: externally mixed LAC and core-shell mixed LAC coated by less absorbing components. The mixing state of ambient aerosol is described by the mass ratio of externally mixed LAC to total LAC:

$$r_{\text{ext-LAC}} = M_{\text{ext-LAC}}/M_{\text{LAC}} \tag{1}$$

where $M_{\text{ext-LAC}}$ is the mass concentration of externally mixed LAC, and M_{LAC} is the total mass concentration of LAC measured by MAAP. According to this assumption,

measured PNSD of aerosol particles is a superposition of the PNSD of externally mixed LAC and the PNSD of core-shell mixed particles:

$$N(\log D_p) = N(\log D_p)_{\text{ext-LAC}} + N(\log D_p)_{\text{core-shell}} \tag{2}$$

where $N(\log D_p)$ is the PNSD measured by TDMPS and APS, $N(\log D_p)_{\text{ext-LAC}}$ and $N(\log D_p)_{\text{core-shell}}$ are the PNSDs of the externally mixed LAC and the core-shell mixed particles, respectively. With the mixing state retrieved by Ma et al. (2012), $N(\log D_p)_{\text{ext-LAC}}$ can be derived using the following equation:

$$N(\log D_p)_{\text{ext-LAC}} = N(\log D_p) \times r_{\text{ext-LAC}} \times f_{\text{LAC}} \tag{3}$$

where f_{LAC} is the volume fraction of LAC, which can be calculated as:

$$f_{\text{LAC}} = \frac{M_{\text{LAC}}}{\rho_{\text{LAC}} \times \sum\limits_{D_p} N(\log D_p) \times (\frac{\pi}{6} \times D_p^3)} \tag{4}$$

where ρ_{LAC} is the density of LAC, which is assumed to be $1.5\,\text{g cm}^{-3}$. Details about the method of retrieving the mixing state of LAC in the NCP can be found in Ma et al. (2012).

To account for the hygroscopic growth of aerosol particles, we define the growth factor as follow:

$$g(D_{p,\,\text{dry}}, \text{RH}) = D_p(\text{RH})/D_{p,\,\text{dry}} \tag{5}$$

where $D_{p,\,\text{dry}}$ and $D_p(\text{RH})$ is the diameter of particle at dry state and specific RH, respectively. The externally mixed LAC is assumed to be completely hydrophobic and does not grow with the increasing RH. The size-resolved hygroscopic growth factor of core-shell mixed particles are calculated using the κ-theory (Petters and Kreidenweis, 2007) to get the PNSD at ambient conditions:

$$\text{RH} = \frac{g^3 - 1}{g^3 - (1 - \kappa)} \times \exp\left(\frac{4\sigma_{\text{s/a}} \times M_{\text{water}}}{R \times T \times D_p \times g}\right) \tag{6}$$

345

where $\sigma_{s/a}$ is the surface tension of solution/air interface, T is the temperature, M_{water} is the molecular weight of water, and R is the universal gas constant. By solving Eq. (6), $g(D_{p,\,dry}, RH)$ at different RH and D_p can be obtained. More information about the size-resolved κ can be found in (Chen et al., 2012; Tao et al., 2014).

To use BHCOAT (Bohren and Huffman, 2008; Cheng et al., 2009) code for the Mie calculation, we need the diameters and complex refractive indices of the core and the shell. For core-shell mixed particles, the diameter of the core does not change as the RH changes and can be calculated using the following equation:

$$D_{core} = D_{p,\,dry} \left(\frac{f_{LAC} - f_{LAC} \times r_{ext\text{-}LAC}}{1 - f_{LAC} \times r_{ext\text{-}LAC}} \right)^{\frac{1}{3}} \tag{7}$$

The complex refractive index of core is set to be $1.96 - 0.66i$ (Seinfeld and Pandis, 2006). However, the shells of aerosol particles will take up water as a function of RH and be dissolved. Both the diameters and complex refractive indices of shells will change, and the complex refractive indices of shells are calculated with the following equation:

$$\widetilde{m}_{shell} = f_{solute} \times \widetilde{m}_{solute} + (1 - f_{solute}) \times \widetilde{m}_{water} \tag{8}$$

Where the volume fraction of solute, f_{solute} follows:

$$f_{solute} = \frac{D_{p,\,dry}^3 - D_{core}^3}{D_p^3(RH) - D_{core}^3} \tag{9}$$

where $\widetilde{m}_{shell}$, $\widetilde{m}_{solute}$, $\widetilde{m}_{water}$ are respectively the complex refractive indices of the shell, solute (assumed to be $1.53 - 10^{-7}i$, Wex et al., 2002), and water (i.e. $1.33 - 10^{-7}i$, Seinfeld and Pandis, 2006).

The SSA is defined as the ratio of the scattering coefficient to the extinction coefficient of aerosol particles. The scattering and absorption coefficients were calculated

from the integration of the corresponding scattering and absorption efficiencies (Q_{sp} and Q_{ap}) over the whole number size distribution:

$$\sigma_{sp/ap} = \int_0^{D_p^{max}} Q_{sp/ap} \times \left(\frac{\pi}{4}D_p^2\right) \times N(\log D_p) \times d\log D_p \qquad (10)$$

where Q_{sp} and Q_{ap} can be calculated through the BHCOAT code. Using Eq. (10), the σ_{sp} and σ_{ap} of externally mixed LAC and core-shell mixed aerosol particles can be calculated individually, and then added up to the total σ_{sp} and σ_{ap}. Finally, SSA can be calculated according to the definition.

To calculate the g of aerosol particles, the following equation (D'Almeida et al., 1991) is used:

$$g = \frac{\sum_i g^i_{ext\text{-}LAC}\sigma^i_{sp,\,ext\text{-}LAC} + g^i_{core\text{-}shell}\sigma^i_{sp,\,core\text{-}shell}}{\sum_i \sigma^i_{sp,\,ext\text{-}LAC} + \sigma^i_{sp,\,core\text{-}shell}} \qquad (11)$$

where i represents the aerosol size bin, $\sigma^i_{sp,\,ext\text{-}LAC}$ and $\sigma^i_{sp,\,core\text{-}shell}$ is respectively the scattering coefficient of externally mixed LAC and core-shell mixed aerosol particles at corresponding size. $g^i_{ext\text{-}LAC}$ and $g^i_{core\text{-}shell}$ is respectively the g of externally mixed LAC and core-shell mixed aerosol at each size bin, which can be calculated using the BHCOAT code.

3.2 Calculation of DARF and case design

The calculated aerosol optical properties are used to evaluate the impacts of their diurnal changes on the estimates of daily average DARF. The temporal resolution of SSA and g is about 10 min, and hourly average data are used as inputs for radiative transfer model. Some cases are designed to evaluate the impact of diurnal variability of aerosol optical properties on the estimates of daily average DARF.

3.2.1 Calculation of direct aerosol radiative forcing

DARF is either evaluated at the TOA or at the surface according to the following equation:

$$F = (f_a \downarrow - f_a \uparrow) - (f_0 \downarrow - f_0 \uparrow) \tag{12}$$

In this expression, F is the DARF, and f denotes the downward/upward irradiance which spans 0.25 µm to 4 µm. ($f \downarrow - f \uparrow$) denotes the net irradiance computed with a given aerosol f_a, or without aerosol f_0, at either the TOA or surface.

The radiative transfer simulations are performed with the Santa Barbara DISORT (discrete ordinates radiative transfer) Atmospheric Radiative Transfer (SBDART) model (Ricchiazzi et al., 1998). We calculated DARF using the derived SSA and g with diurnal pattern of AOD from an AERONET site, Xianghe. The Angström exponents calculated with the aerosol extinction coefficient at 470 and 860 nm are used to account for the spectral dependence of AOD. Moreover, SSA and g at four wavelengths (470, 550, 860 and 1240 nm) are used as input of the SBDART model. The atmospheric profile of Mid-Latitude summer provided by SBDART itself is used in simulations. The information of surface albedo is obtained from MCD43C3 albedo product (https://lpdaac.usgs.gov/products/modis_products_table/mcd43c3). To obtain the daily average DARF, the calculations are performed with a one-hour time step from local time 06:00 to 18:00.

3.2.2 Case design

Several cases are designed to evaluate the impacts of the diurnal variations of aerosol optical properties on the daily average DARF. The designed cases are listed in Table 1. The abbreviation abt stands for ambient. $\overline{dt}$, $\overline{am}$ and $\overline{pm}$ and $\overline{ap}$ indicate that the aerosol optical properties are averaged over four different time periods: daytime, early morning, late afternoon, and both early morning and late afternoon. Early morning is defined by the period when SZA is within 50 and 70° in the morning. Late afternoon is defined by

the period when SZA is within 50 and 70° in the afternoon. This specified early morning and late afternoon periods mimic the AERONET sampling periods used for retrieving SSA and g (Kassianov et al., 2013). Among all these cases, Case 1 is supposed to be the reference case because SSA and g in Case 1 are both for ambient condition with the diurnal changes of AOD also considered. Case 2 is designed to study the impacts of the daily averages of AOD, SSA and g on the DARF. Cases 3 to 8 are designed to investigate the sensitivity of daily average DARF to the diurnal changes of AOD, SSA and g. Cases 9 to 11 are designed to test how the daily average DARF responds if the SSA and g are both averaged over either early morning, late afternoon or both early morning and late afternoon. For Cases 2 to 11, the actual diurnal variations of aerosol optical properties are ignored, and the corresponding averages are used instead.

To estimate the difference between a specified case and the reference case, we define the relative difference (RD) as follow:

$$\text{RD} = \frac{F_{case} - F_{case1}}{F_{case1}} \times 100\,\% \tag{13}$$

where F_{case} is the daily average DARF at TOA/surface of specified case, F_{case1} is the daily average DARF at TOA/surface of Case 1.

4 Results and discussions

4.1 Diurnal variations of aerosol optical properties

The diurnal variation of AOD at 550 nm in Xianghe summer is presented in Fig. 1. AOD at 550 nm is calculated using the AOD at 500 nm and the Ångström exponent between 440 and 675 nm provided by AERONET AOD product. Like Wuqing, Xianghe is also a background site of the NCP, the distance between them is about 40 km. The daily average AOD at 550 nm is 0.47, which means that the NCP is highly polluted.

AOD shows two peaks in the morning and the afternoon, respectively, and the relative departures of AOD from daily mean can be up to 20 % on average.

Using the method mentioned in Sect. 3, SSA and g are calculated from the observation. The obtained SSA and g have a temporal resolution of about ten minutes, and are averaged to one-hour data to show their diurnal variations. Those days without a full temporal coverage of SSA or g are excluded, thus, 17 days are available. Only the local time range from 06:00 to 18:00 is considered, since the direct interaction of aerosol with the solar shortwave radiation only happens during daytime.

SSA is very important for the accurate estimation of DARF (McComiskey et al., 2008). But the diurnal variation of SSA for ambient aerosol is rarely studied, especially in the NCP, due to limitations exist in current methods for obtaining SSA. The average diurnal variations of SSA for the ambient and the dry state aerosols during the observation period are illustrated in Fig. 2. It can be seen from the graph that the diurnal pattern of SSA at the two states are far different. At dry conditions, the SSA reaches minimum in the morning and evening, and maximum at noon, with an average of 0.84. This result is similar to most previous studies on the diurnal variation of SSA for dry state aerosol (He et al., 2009; Fan et al., 2010; Junwei et al., 2012; Gyawali et al., 2012). For ambient aerosol, many of the aerosol components are hygroscopic and can take up water as a function of RH (Bian et al., 2014; Cheng et al., 2008), making the SSA change as the RH changes. In this study, our results demonstrate that the diurnal variation of SSA for ambient aerosol is evident. The SSA reaches maximum in the morning when RH is the highest and minimum in the afternoon, difference between the maximum and minimum can be up to 0.06, with the average at 0.90. Due to the hygroscopic growth of aerosol particles, the scattering coefficient will be largely enhanced when RH is greater than 60 % (Cheng et al., 2008). However, the dependence of aerosol absorption on RH is not as significant as that of scattering (Redemann et al., 2001; Tao et al., 2014). According to the definition of SSA, its diurnal variation will be largely influenced by RH, especially when RH is high. The average diurnal pattern of RH during the corresponding period is shown in Fig. 3. RH begins to decrease in the

Title Page

Abstract | Introduction

Conclusions | References

Tables | Figures

◀ | ▶

◀ | ▶

Back | Close

Full Screen / Esc

Printer-friendly Version

Interactive Discussion

morning at 06:00, and reaches minimum in the afternoon. And the RH during this observation period is frequently higher than 60 %. Hence, it can be seen from Fig. 2 that the diurnal pattern of SSA for ambient aerosol is dominated by but not completely consistent with that of RH. Due to the RH in the afternoon is not high enough, and the SSA of dry state aerosol will play a role. But the diurnal pattern of the ratio between the SSA of ambient and dry state aerosol is highly correlated with that of RH, and the daily average ratio is 1.07.

For g, it is also an important parameter for estimating DARF (McComiskey et al., 2008), the characteristics of its diurnal variation is rarely investigated, especially in the NCP, due to the difficulty of direct observation of g for ambient aerosol. The average diurnal patterns of g for dry state aerosol and ambient aerosol during the observation period are also illustrated in Fig. 2. It is obvious that the diurnal changes of g at two states are quite different. The g of dry state aerosol shows little variability during daytime, and its daily average is 0.61. On the contrary, g of ambient aerosol has evident diurnal variation. Like SSA, the g reaches maximum in the morning when RH is the highest and minimum in the afternoon when RH is the lowest, difference between the maximum and minimum can be up to 0.1, with the average at 0.69. The diurnal pattern of g for ambient aerosol is highly correlated with that of RH. The diurnal pattern of the ratio between g of ambient and dry state aerosol is also consistent with that of RH, and the daily average ratio is 1.12. This can be easily understood, because g of dry state aerosol has no obvious diurnal variation, the diurnal pattern of g for ambient aerosol is mainly dominated by the diurnal pattern of RH.

4.2 The impacts of diurnal variations of aerosol optical properties on the estimation of daily average DARF

The average diurnal pattern of AOD, SSA and g introduced in Sect. 4.1 are used to estimate the overall influence of their diurnal changes on the estimation of DARF. The influences at TOA and surface are evaluated separately, and the designed cases are introduced in Sect. 3.2.2. Results of this assessment are shown in Figs. 4 and 5, cor-

responding to TOA and surface respectively. The results of Case 2 at TOA and surface demonstrate that an accurate prediction of daily average DARF can be achieved by using the daily averages of AOD, SSA and g, even when their diurnal variations are all evident. For Case 3, it leads to an overestimation of the negative daily average DARF at TOA and surface, due to the overestimation of AOD averaged over early morning. This means, if the temporal coverage of AOD is incomplete, it might result in a large bias in the estimation of daily average DARF at TOA and surface when the diurnal variation of AOD is significant. A similar conclusion is reached from previous studies (Arola et al., 2013; Kassianov et al., 2013). In Cases 5 and 6, the SSA averaged over the early morning or late afternoon is used. As a result, the estimated daily average DARF shows large biases. A larger SSA will cause less absorbing of incident solar radiation by atmospheric aerosol, more light hit onto the ground and reflected into space. The overestimation of SSA in the early morning will therefore result in a stronger negative radiative forcing (NRF) at TOA and weaker NRF at surface. In Cases 7 and 8, the g averaged over the early morning or late afternoon is used, it will also lead to large biases in the estimation of daily average DARF at TOA. With the increase of g, more light will be forward scattered, absorbed by the atmospheric aerosol, and hit onto the ground. Consequently, the overestimation of g in the early morning will result in weaker NRF at TOA and surface. The results from Cases 5 to 8 indicate the diurnal variations of SSA and g in the NCP have significant impacts on the estimation of DARF at TOA, but less impacts on the estimation of DARF at surface. If the temporal resolution of SSA and g is not high enough to accurately represent their diurnal variations, the estimated daily average DARF at TOA might be biased significantly.

As mentioned in the introduction, currently, the measurements from AERONET and satellites are widely used in the estimation of DARF. But the irregular sampling of aerosol optical properties from those measurements may be unable to faithfully capture their diurnal changes. It is necessary to find if it is possible to improve the estimation of daily average DARF for data with incomplete temporal coverage of these diurnal changes. AOD from satellites and ground-based measurements are usually used in the

estimation of daily averaged DARF. For ground-based measurements particularly, it is possible to accurately capture the diurnal variation of AOD. For SSA and g, the measurements from AERONET are widely used in the estimation of daily average DARF. However, their retrievals from AERONET measurements are typically limited to rela-
5 tively short periods in the early morning and late afternoon when the SZA is quite large ($50° \leq$ SZA $\leq 70°$) (Dubovik et al., 2000; Holben et al., 2006). In view of this, Cases 9 to 11 are designed to test the performance of different cases in order to find some suggestions about the estimation of daily average DARF when the temporal samplings of SSA and g are incomplete.
10 In Case 9, the SSA and g are both averaged over early morning, and daily average AOD is used. The results show that this treatment has less influence on the estimation of daily average DARF at TOA, but larger influences at surface than in Cases 5 and 7. According to the analysis of Cases 5 to 8, the overestimation of SSA will lead to stronger NRF at TOA and weaker NRF at surface. The overestimation of g will result in
15 weaker NRF at TOA and surface. The effect of the overestimation of SSA and g will be cancelled out to some extent at TOA, but enhanced at the surface, and vice versa in Case 10. In Case 11, the results demonstrate that both SSA and g averaged over early morning and late afternoon only has little influence on the estimation of daily average DARF at TOA and surface. Conclusions can be made that, overall, for estimating DARF
20 at TOA, schemes of Cases 9 to 11 can largely improve the results compare to Cases 5 to 8. Case 11 is the best and also suitable for estimating DARF at surface.

The results of cases at TOA for individual days with specific diurnal variations of SSA and g are shown in Fig. 6. The diurnal pattern of AOD for all days is fixed, and is the same as the one introduced in Sect. 4.1. Overall, the results from cases for
25 different days are consistent with the results from cases aforementioned. In particular, the results of Case 11 are very stable and close to the results of Case 2. This means that, even if the diurnal variations of SSA and g are not in exactly accordance with the average pattern mentioned in Sect. 4.1, the scheme of Case 11 still can lead to a good result. But exception still exists for Case 11, the relative difference in Julian day

of 197 is notably larger than that in other days, and the least improvement compare to results of other cases. It is found that the diurnal variation of RH at this day is far different from the one introduced in Sect. 4.1. The diurnal variations of SSA, g and RH at Julian day of 197 are shown in Fig. 7. It's clear that the diurnal variations of SSA

5 and g are dominated by the diurnal variation of RH, but not like their typical pattern in those selected days. There are two reasons that the results of Case 11 are very small and stable in most of days. First, the diurnal pattern of SSA and g are both dominated by the diurnal variation of RH, thus the SSA and g are both highest in the morning and lowest in the afternoon, the SSA and g averaged over early morning and late afternoon

10 will be closer to their daily averages than Cases 9 and 10. Second, according to the analysis for the results of Cases 9 and 10, the SSA and g have opposite effects on the estimation of daily averaged DARF at TOA, the influence of SSA will be offset to some extent by that of g. Therefore, the diurnal pattern of RH is an important factor which determines if the scheme of Case 11 can be used to improve the estimation

15 of daily average DARF. On the other hand, the results of Cases 9 and 10 are not as stable as that of Case 11, but still much better than those of Cases 5 to 8. The diurnal pattern of RH shown in Fig. 4 is prevalent in different regions and seasons around the world (Ephrath et al., 1996; Gebhart et al., 2001; Fan et al., 2010; Sun et al., 2013; Li et al., 2013), the scheme of Case 11 maybe also suitable for different regions. We

20 suggest that using the scheme of Case 11 to improve the accurate estimation of DARF. If the temporal samplings of SSA and g are too few to adopt the scheme of Case 11, schemes of Cases 9 and 10 still can be good options for improving the estimation of DARF at TOA.

5 Conclusions

25 SSA and g are both important parameters in the estimation of DARF (McComiskey et al., 2008), but their diurnal variations are rarely investigated, especially in the NCP. In this paper, using the in-situ measurements from HaChi campaign, the diurnal varia-

tions of SSA and g are studied. The results show that, for ambient aerosol, the diurnal variations of SSA and g are both evident, and far different from those of dry state aerosol. For dry state aerosol, the SSA reaches minimum in the morning and evening, and maximum at noon, with the average at 0.84. For ambient aerosol, the SSA reaches maximum in the morning when RH is the highest and minimum in the afternoon, difference between the maximum and minimum can be up to 0.06, with the average at 0.90. The diurnal pattern of SSA for ambient aerosol is dominated by that of RH, and the average ratio between the SSA of ambient and dry state aerosol is 1.07. On the other hand, the g of dry state aerosol shows little variability during daytime, with an average of 0.61. The diurnal pattern of g for ambient aerosol is also evident and dominated by that of RH, the difference between the maximum and minimum can be up to 0.1, with an average of 0.69. The average ratio of g for ambient aerosol to that for dry state aerosol is 1.12.

Using the SSA and g calculated from in-situ measurements, and AOD from AERONET measurements, several cases are designed to evaluate the impacts of the diurnal changes of AOD, SSA and g on the estimates of daily average DARF. The results demonstrate that the diurnal changes of SSA and g in the NCP have significant influence on the estimation of DARF at TOA, which means that if the temporal samplings of SSA and g are incomplete, significant errors may occur in the estimation of DARF at TOA. If the full temporal coverage of AOD, SSA and g are available, the accurate estimation of DARF can be achieved by using the daily averages of AOD, SSA and g. However, due to the lack of full temporal coverage datasets of SSA and g, their daily averages are usually not available. Regarding this, three cases are designed in order to find some suggestions about the estimation of daily average DARF. We conclude that, if the RH plays a dominant role in the diurnal variations of SSA and g, an accurate estimation of DARF can be achieved by using SSA and g averaged over early morning and late afternoon as inputs for radiative transfer model. If the samplings of SSA or g are only available in the early morning or late afternoon, either averaged over early morning or late afternoon of both SSA and g can be used to improve the estimation of

DARF at TOA. Those important findings may allow one to bypass the complex temporal monitoring problems associated with significant diurnal changes of SSA and g. This study will further our understanding of the diurnal characteristics of SSA and g in the NCP and help for improving the accurate estimation of DARF.

References

Arola, A., Eck, T. F., Huttunen, J., Lehtinen, K. E. J., Lindfors, A. V., Myhre, G., Smirnov, A., Tripathi, S. N., and Yu, H.: Influence of observed diurnal cycles of aerosol optical depth on aerosol direct radiative effect, Atmos. Chem. Phys., 13, 7895–7901, doi:10.5194/acp-13-7895-2013, 2013.

Bellouin, N., Boucher, O., Haywood, J., and Reddy, M. S.: Global estimate of aerosol direct radiative forcing from satellite measurements, Nature, 438, 1138–1141, 2005.

Bellouin, N., Jones, A., Haywood, J., and Christopher, S. A.: Updated estimate of aerosol direct radiative forcing from satellite observations and comparison against the Hadley Centre climate model, J. Geophys. Res.-Atmos., 113, D10205, doi:10.1029/2007JD009385, 2008.

Bellouin, N., Quaas, J., Morcrette, J.-J., and Boucher, O.: Estimates of aerosol radiative forcing from the MACC re-analysis, Atmos. Chem. Phys., 13, 2045–2062, doi:10.5194/acp-13-2045-2013, 2013.

Bian, Y. X., Zhao, C. S., Ma, N., Chen, J., and Xu, W. Y.: A study of aerosol liquid water content based on hygroscopicity measurements at high relative humidity in the North China Plain, Atmos. Chem. Phys., 14, 6417–6426, doi:10.5194/acp-14-6417-2014, 2014.

Birmili, W., Stratmann, F., and Wiedensohler, A.: Design of a DMA-based size spectrometer for a large particle size range and stable operation, J. Aerosol Sci., 30, 549–553, doi:10.1016/s0021-8502(98)00047-0, 1999.

Bohren, C. F. and Huffman, D. R.: Absorption and Scattering of Light by Small Particles, Wiley, com, New York, USA, 2008.

Title Page

Abstract | Introduction

Conclusions | References

Tables | Figures

Back | Close

Full Screen / Esc

Printer-friendly Version

Interactive Discussion

Bond, T. C., Doherty, S. J., Fahey, D., Forster, P., Berntsen, T., DeAngelo, B., Flanner, M., Ghan, S., Kärcher, B., and Koch, D.: Bounding the role of black carbon in the climate system: a scientific assessment, J. Geophys. Res.-Atmos., 118, 5380–5552, 2013.

Chen, J., Zhao, C. S., Ma, N., Liu, P. F., Göbel, T., Hallbauer, E., Deng, Z. Z., Ran, L., Xu, W. Y., Liang, Z., Liu, H. J., Yan, P., Zhou, X. J., and Wiedensohler, A.: A parameterization of low visibilities for hazy days in the North China Plain, Atmos. Chem. Phys., 12, 4935–4950, doi:10.5194/acp-12-4935-2012, 2012.

Cheng, Y., Wiedensohler, A., Eichler, H., Heintzenberg, J., Tesche, M., Ansmann, A., Wendisch, M., Su, H., Althausen, D., and Herrmann, H.: Relative humidity dependence of aerosol optical properties and direct radiative forcing in the surface boundary layer at Xinken in Pearl River Delta of China: an observation based numerical study, Atmos. Environ., 42, 6373–6397, 2008.

Cheng, Y. F., Berghof, M., Garland, R. M., Wiedensohler, A., Wehner, B., Muller, T., Su, H., Zhang, Y. H., Achtert, P., Nowak, A., Poschl, U., Zhu, T., Hu, M., and Zeng, L. M.: Influence of soot mixing state on aerosol light absorption and single scattering albedo during air mass aging at a polluted regional site in northeastern China, J. Geophys. Res.-Atmos., 114, D00G10, doi:10.1029/2008jd010883, 2009.

Chung, C. E., Ramanathan, V., Kim, D., and Podgorny, I. A.: Global anthropogenic aerosol direct forcing derived from satellite and ground-based observations, J. Geophys. Res.-Atmos., 110, D24207, doi:10.1029/2005jd006356, 2005.

D'Almeida, G. A., Koepke, P., and Shettle, E. P.: Atmospheric Aerosols: Global Climatology and Radiative Characteristics, A. Deepak Pub., Hampton, Va, 1991.

Dubovik, O., Smirnov, A., Holben, B., King, M., Kaufman, Y., Eck, T., and Slutsker, I.: Accuracy assessments of aerosol optical properties retrieved from Aerosol Robotic Network (AERONET) Sun and sky radiance measurements, J. Geophys. Res.-Atmos., 105, 9791–9806, 2000.

Ephrath, J. E., Goudriaan, J., and Marani, A.: Modelling diurnal patterns of air temperature, radiation wind speed and relative humidity by equations from daily characteristics, Agr. Syst., 51, 377–393, doi:10.1016/0308-521X(95)00068-G, 1996.

Fan, X., Chen, H., Xia, X., Li, Z., and Cribb, M.: Aerosol optical properties from the Atmospheric Radiation Measurement Mobile Facility at Shouxian, China, J. Geophys. Res.-Atmos., 115, D00K33, doi:10.1029/2010jd014650, 2010.

Gebhart, K. A., Copeland, S., and Malm, W. C.: Diurnal and seasonal patterns in light scattering, extinction, and relative humidity, Atmos. Environ., 35, 5177–5191, doi:10.1016/S1352-2310(01)00319-3, 2001.

Gyawali, M., Arnott, W. P., Zaveri, R. A., Song, C., Moosmüller, H., Liu, L., Mishchenko, M. I., Chen, L.-W. A., Green, M. C., Watson, J. G., and Chow, J. C.: Photoacoustic optical properties at UV, VIS, and near IR wavelengths for laboratory generated and winter time ambient urban aerosols, Atmos. Chem. Phys., 12, 2587–2601, doi:10.5194/acp-12-2587-2012, 2012.

He, X., Li, C. C., Lau, A. K. H., Deng, Z. Z., Mao, J. T., Wang, M. H., and Liu, X. Y.: An intensive study of aerosol optical properties in Beijing urban area, Atmos. Chem. Phys., 9, 8903–8915, doi:10.5194/acp-9-8903-2009, 2009.

Hennig, T., Massling, A., Brechtel, F. J., and Wiedensohler, A.: A tandem DMA for highly temperature-stabilized hygroscopic particle growth measurements between 90 % and 98 % relative humidity, J. Aerosol Sci., 36, 1210–1223, doi:10.1016/j.jaerosci.2005.01.005, 2005.

Holben, B., Eck, T., Slutsker, I., Tanre, D., Buis, J., Setzer, A., Vermote, E., Reagan, J., Kaufman, Y., and Nakajima, T.: AERONET – a federated instrument network and data archive for aerosol characterization, Remote Sens. Environ., 66, 1–16, 1998.

Holben, B. N., Eck, T. F., Slutsker, I., Smirnov, A., Sinyuk, A., Schafer, J., Giles, D., and Dubovik, O.: Aeronet's Version 2.0 quality assurance criteria, Proc. SPIE 6408, Remote Sensing of the Atmosphere and Clouds, 64080Q, doi:10.1117/12.706524, 2006.

Junwei, X., Jun, T., Renjian, Z., Tiantao, C., Chunpeng, L., Jianmin, C., Guanghan, H., Xiang, L., and Zhaoqin, Z.: Measurements of surface aerosol optical properties in winter of Shanghai, Atmos. Res., 109, 25–35, doi:10.1016/j.atmosres.2012.02.008, 2012.

Kassianov, E., Barnard, J., Pekour, M., Berg, L. K., Michalsky, J., Lantz, K., and Hodges, G.: Do diurnal aerosol changes affect daily average radiative forcing?, Geophys. Res. Lett., 40, 3265–3269, doi:10.1002/grl.50567, 2013.

Li, C., Tsay, S. C., Hsu, N. C., Kim, J. Y., Howell, S. G., Huebert, B. J., Ji, Q., Jeong, M. J., Wang, S. H., Hansell, R. A., and Bell, S. W.: Characteristics and composition of atmospheric aerosols in Phimai, central Thailand during BASE-ASIA, Atmos. Environ., 78, 60–71, doi:10.1016/j.atmosenv.2012.04.003, 2013.

Liu, P. F., Zhao, C. S., Göbel, T., Hallbauer, E., Nowak, A., Ran, L., Xu, W. Y., Deng, Z. Z., Ma, N., Mildenberger, K., Henning, S., Stratmann, F., and Wiedensohler, A.: Hygroscopic properties of aerosol particles at high relative humidity and their diurnal variations in the North China Plain, Atmos. Chem. Phys., 11, 3479–3494, doi:10.5194/acp-11-3479-2011, 2011.

Title Page

Abstract | Introduction

Conclusions | References

Tables | Figures

|◀ | ▶|

◀ | ▶

Back | Close

Full Screen / Esc

Printer-friendly Version

Interactive Discussion

Ma, N., Zhao, C. S., Nowak, A., Müller, T., Pfeifer, S., Cheng, Y. F., Deng, Z.Z., Liu, P. F., Xu, W. Y., Ran, L., Yan, P., Göbel, T., Hallbauer, E., Mildenberger, K., Henning, S., Yu, J., Chen, L. L., Zhou, X. J., Stratmann, F., and Wiedensohler, A.: Aerosol optical properties in the North China Plain during HaChi campaign: an in-situ optical closure study, Atmos. Chem. Phys., 11, 5959–5973, doi:10.5194/acp-11-5959-2011, 2011.

Ma, N., Zhao, C. S., Müller, T., Cheng, Y. F., Liu, P. F., Deng, Z. Z., Xu, W. Y., Ran, L., Nekat, B., van Pinxteren, D., Gnauk, T., Müller, K., Herrmann, H., Yan, P., Zhou, X. J., and Wieden- sohler, A.: A new method to determine the mixing state of light absorbing carbonaceous using the measured aerosol optical properties and number size distributions, Atmos. Chem. Phys., 12, 2381–2397, doi:10.5194/acp-12-2381-2012, 2012.

Mazzola, M., Lanconelli, C., Lupi, A., Busetto, M., Vitale, V., and Tomasi, C.: Columnar aerosol optical properties in the Po Valley, Italy, from MFRSR data, J. Geophys. Res.-Atmos., 115, D17206, doi:10.1029/2009jd013310, 2010.

McComiskey, A., Schwartz, S. E., Schmid, B., Guan, H., Lewis, E. R., Ricchiazzi, P., and Ogren, J. A.: Direct aerosol forcing: calculation from observables and sensitivities to inputs, J. Geophys. Res.-Atmos., 113, D09202, doi:10.1029/2007JD009170, 2008.

Myhre, G.: Consistency between satellite-derived and modeled estimates of the direct aerosol effect, Science, 325, 187–190, 2009.

Myhre, G., Samset, B. H., Schulz, M., Balkanski, Y., Bauer, S., Berntsen, T. K., Bian, H., Bellouin, N., Chin, M., Diehl, T., Easter, R. C., Feichter, J., Ghan, S. J., Hauglustaine, D., Iversen, T., Kinne, S., Kirkevåg, A., Lamarque, J.-F., Lin, G., Liu, X., Lund, M. T., Luo, G., Ma, X., van Noije, T., Penner, J. E., Rasch, P. J., Ruiz, A., Seland, Ø., Skeie, R. B., Stier, P., Takemura, T., Tsigaridis, K., Wang, P., Wang, Z., Xu, L., Yu, H., Yu, F., Yoon, J.-H., Zhang, K., Zhang, H., and Zhou, C.: Radiative forcing of the direct aerosol effect from AeroCom Phase II simulations, Atmos. Chem. Phys., 13, 1853–1877, doi:10.5194/acp-13-1853-2013, 2013.

Petters, M. D. and Kreidenweis, S. M.: A single parameter representation of hygroscopic growth and cloud condensation nucleus activity, Atmos. Chem. Phys., 7, 1961–1971, doi:10.5194/acp-7-1961-2007, 2007.

Ran, L., Zhao, C. S., Xu, W. Y., Lu, X. Q., Han, M., Lin, W. L., Yan, P., Xu, X. B., Deng, Z. Z., Ma, N., Liu, P. F., Yu, J., Liang, W. D., and Chen, L. L.: VOC reactivity and its effect on ozone production during the HaChi summer campaign, Atmos. Chem. Phys., 11, 4657–4667, doi:10.5194/acp-11-4657-2011, 2011.

Title Page

Abstract | Introduction

Conclusions | References

Tables | Figures

◄ | ►

◄ | ►

Back | Close

Full Screen / Esc

Printer-friendly Version

Interactive Discussion

Redemann, J., Russell, P. B., and Hamill, P.: Dependence of aerosol light absorption and single-scattering albedo on ambient relative humidity for sulfate aerosols with black carbon cores, J. Geophys. Res.-Atmos., 106, 27485–27495, doi:10.1029/2001jd900231, 2001.

Remer, L. A. and Kaufman, Y. J.: Aerosol direct radiative effect at the top of the atmosphere over cloud free ocean derived from four years of MODIS data, Atmos. Chem. Phys., 6, 237–253, doi:10.5194/acp-6-237-2006, 2006.

Ricchiazzi, P., Yang, S., Gautier, C., and Sowle, D.: SBDART: a research and teaching software tool for plane-parallel radiative transfer in the Earth's atmosphere, B. Am. Meteorol. Soc., 79, 2101–2114, 1998.

Seinfeld, J. H. and Pandis, S. N.: Atmospheric Chemistry and Physics: From Air Pollution to Climate Change, John Wiley & Sons, New York, USA, 2006.

Sena, E. T., Artaxo, P., and Correia, A. L.: Spatial variability of the direct radiative forcing of biomass burning aerosols and the effects of land use change in Amazonia, Atmos. Chem. Phys., 13, 1261–1275, doi:10.5194/acp-13-1261-2013, 2013.

Smirnov, A., Holben, B. N., Eck, T. F., Slutsker, I., Chatenet, B., and Pinker, R. T.: Diurnal variability of aerosol optical depth observed at AERONET (Aerosol Robotic Network) sites, Geophys. Res. Lett., 29, 2115, doi:10.1029/2002gl016305, 2002.

Su, W., Loeb, N. G., Schuster, G. L., Chin, M., and Rose, F. G.: Global all-sky shortwave direct radiative forcing of anthropogenic aerosols from combined satellite observations and GOCART simulations, J. Geophys. Res.-Atmos., 118, 655–669, 2013.

Sun, Y., Zhou, X., Wai, K., Yuan, Q., Xu, Z., Zhou, S., Qi, Q., and Wang, W.: Simultaneous measurement of particulate and gaseous pollutants in an urban city in North China Plain during the heating period: implication of source contribution, Atmos. Res., 134, 24–34, doi:10.1016/j.atmosres.2013.07.011, 2013.

Tao, J. C., Zhao, C. S., Ma, N., and Liu, P. F.: The impact of aerosol hygroscopic growth on the single-scattering albedo and its application on the NO_2 photolysis rate coefficient, Atmos. Chem. Phys., 14, 12055–12067, doi:10.5194/acp-14-12055-2014, 2014.

Wex, H., Neususs, C., Wendisch, M., Stratmann, F., Koziar, C., Keil, A., Wiedensohler, A., and Ebert, M.: Particle scattering, backscattering, and absorption coefficients: an in situ closure and sensitivity study, J. Geophys. Res.-Atmos., 107, 8112, doi:10.1029/2000jd000234, 2002.

Xu, W. Y., Zhao, C. S., Ran, L., Deng, Z. Z., Liu, P. F., Ma, N., Lin, W. L., Xu, X. B., Yan, P., He, X., Yu, J., Liang, W. D., and Chen, L. L.: Characteristics of pollutants and their correlation to

meteorological conditions at a suburban site in the North China Plain, Atmos. Chem. Phys., 11, 4353–4369, doi:10.5194/acp-11-4353-2011, 2011.

Zhang, Y., Yu, H., Eck, T. F., Smirnov, A., Chin, M., Remer, L. A., Bian, H., Tan, Q., Levy, R., and Holben, B. N.: Aerosol daytime variations over North and South America derived from multiyear AERONET measurements, J. Geophys. Res.-Atmos., 117, D05211, doi:10.1029/2011JD017242, 2012.

Zhao, C., Tie, X., and Lin, Y.: A possible positive feedback of reduction of precipitation and increase in aerosols over eastern central China, Geophys. Res. Lett., 33, L11814, doi:10.1029/2006GL025959, 2006.

Table 1. Designed cases.

	Case 1	Case 2	Case 3	Case 4	Case 5	Case 6	Case 7	Case 8	Case 9	Case 10	Case 11
AOD	abt	$\overline{dt}$	$\overline{am}$	$\overline{pm}$	$\overline{dt}$	$\overline{dt}$	$\overline{dt}$	$\overline{dt}$	$\overline{dt}$	$\overline{dt}$	$\overline{dt}$
SSA	abt	$\overline{dt}$	$\overline{dt}$	$\overline{dt}$	$\overline{am}$	$\overline{pm}$	$\overline{dt}$	$\overline{dt}$	$\overline{am}$	$\overline{pm}$	$\overline{ap}$
g	abt	$\overline{dt}$	$\overline{dt}$	$\overline{dt}$	$\overline{dt}$	$\overline{dt}$	$\overline{am}$	$\overline{pm}$	$\overline{am}$	$\overline{pm}$	$\overline{ap}$

abt: ambient; $\overline{dt}$: averaged over daytime (06:00 to 18:00), $\overline{am}$: averaged over early morning; $\overline{pm}$: averaged over late afternoon; $\overline{ap}$: averaged over early morning and late afternoon; early morning: $50° \leq SZA \leq 70°$ in the morning; late afternoon: $50° \leq SZA \leq 70°$ in the afternoon.
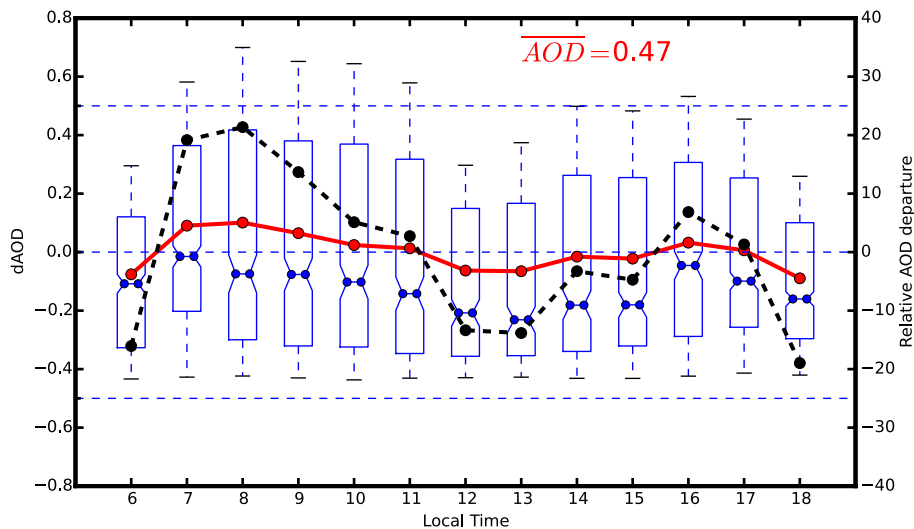
Figure 1. The average diurnal pattern of AOD from AERONET measurements, Xianghe summer. Red line represents the absolute AOD departures (dAOD) from daily mean. Box plots give absolute AOD departure range from 25th to 75th percentile, and bars outside the boxes give the range within 5th to 95th percentile, the blue dots in the box are medians. Black solid points give the relative departures in the right axis.
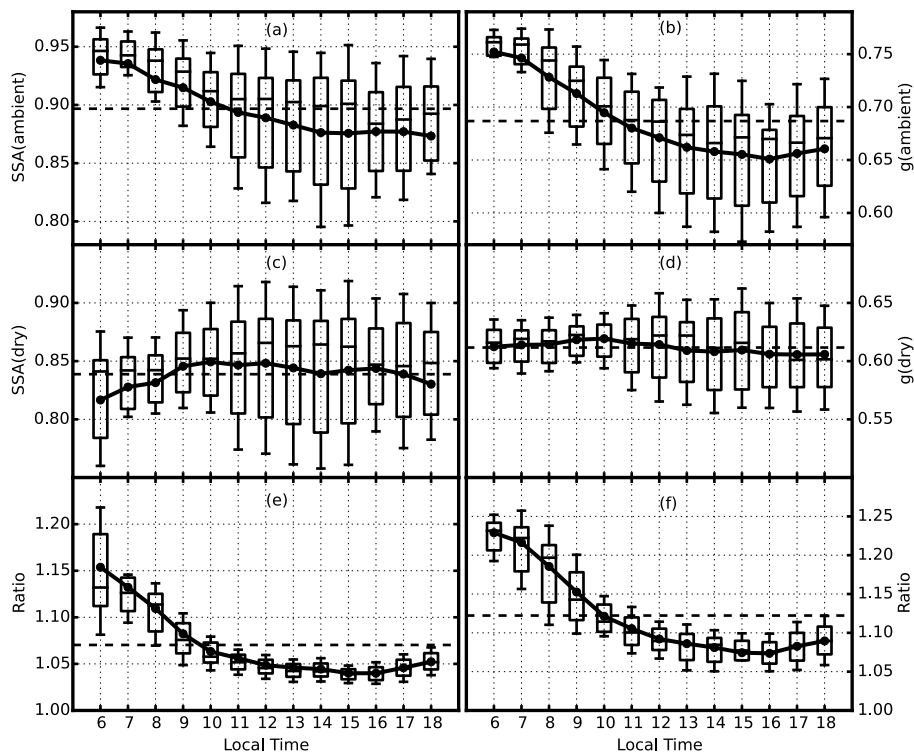
Figure 2. The diurnal variations of SSA and g, **(a)** average diurnal pattern of SSA for ambient aerosol; **(c)** average diurnal pattern of SSA for dry state aerosol; **(e)** the ratio between **(a)** and **(c)**; **(b)** average diurnal pattern of g for ambient aerosol; **(d)** average diurnal pattern of g for dry state aerosol, **(f)** the ratio between **(b)** and **(d)**. Black lines are the average diurnal variations, and dashed lines are their corresponding averages. Box plots give the data points range from 25th to 75th percentile, and bars outside the boxes give the range within 5th to 95th percentile. Lines in boxes are medians.
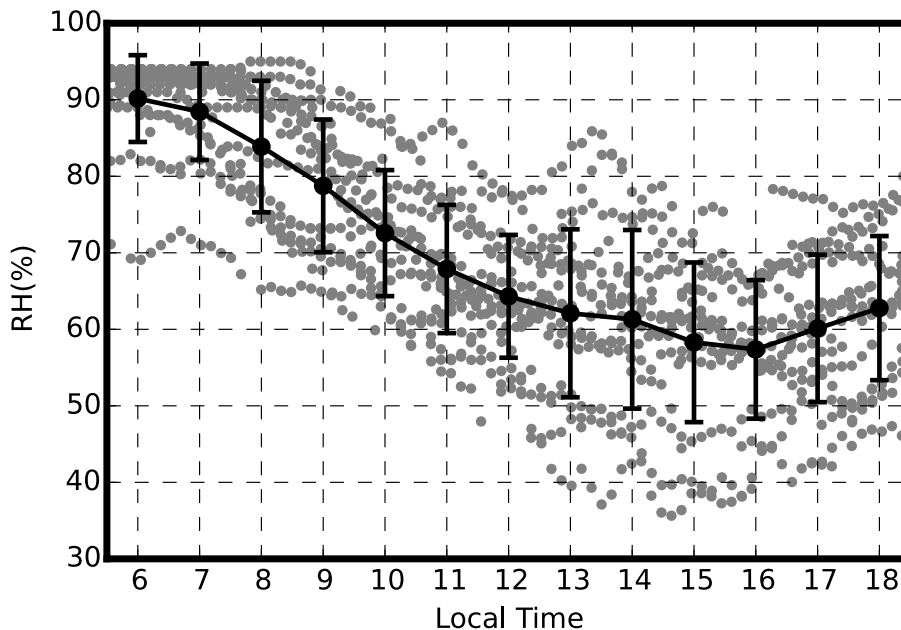
Figure 3. The scatter plots of RH for selected days, the black line is the average diurnal variation of RH.
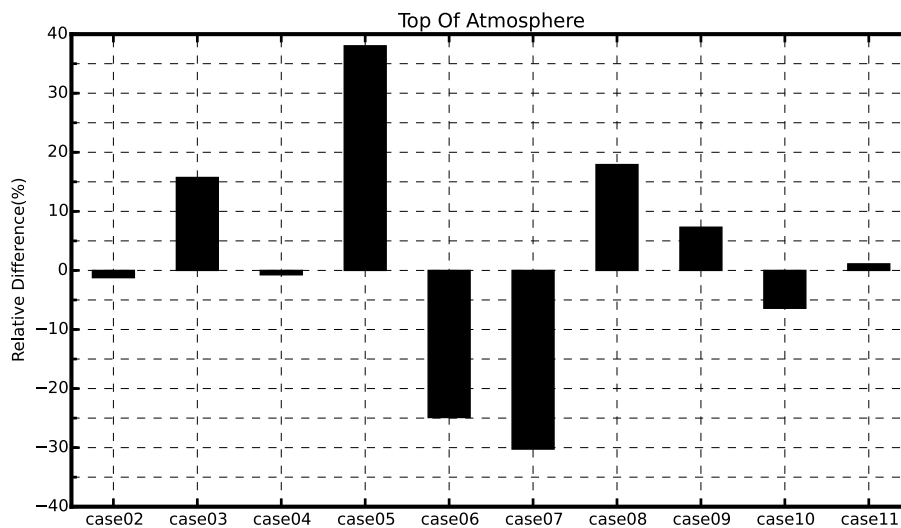
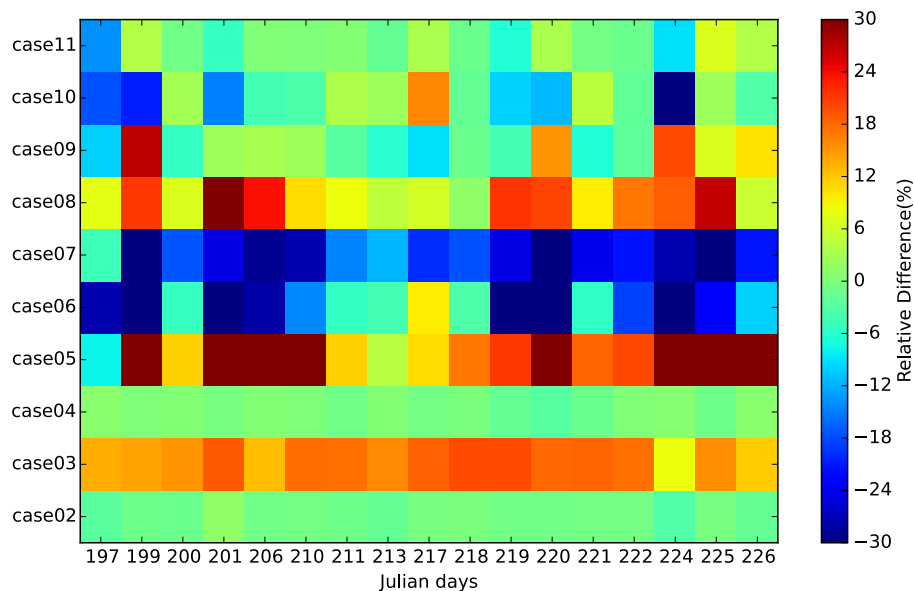**Figure 4.** Relative differences compare to Case 1 of different cases at TOA.

Title Page

Abstract | Introduction

Conclusions | References

Tables | Figures

Back | Close

Full Screen / Esc

Printer-friendly Version

Interactive Discussion

Figure 5. Relative differences compare to Case 1 of different cases at surface.

Figure 6. The relative differences compare to Case 1 of different cases for different days at TOA.
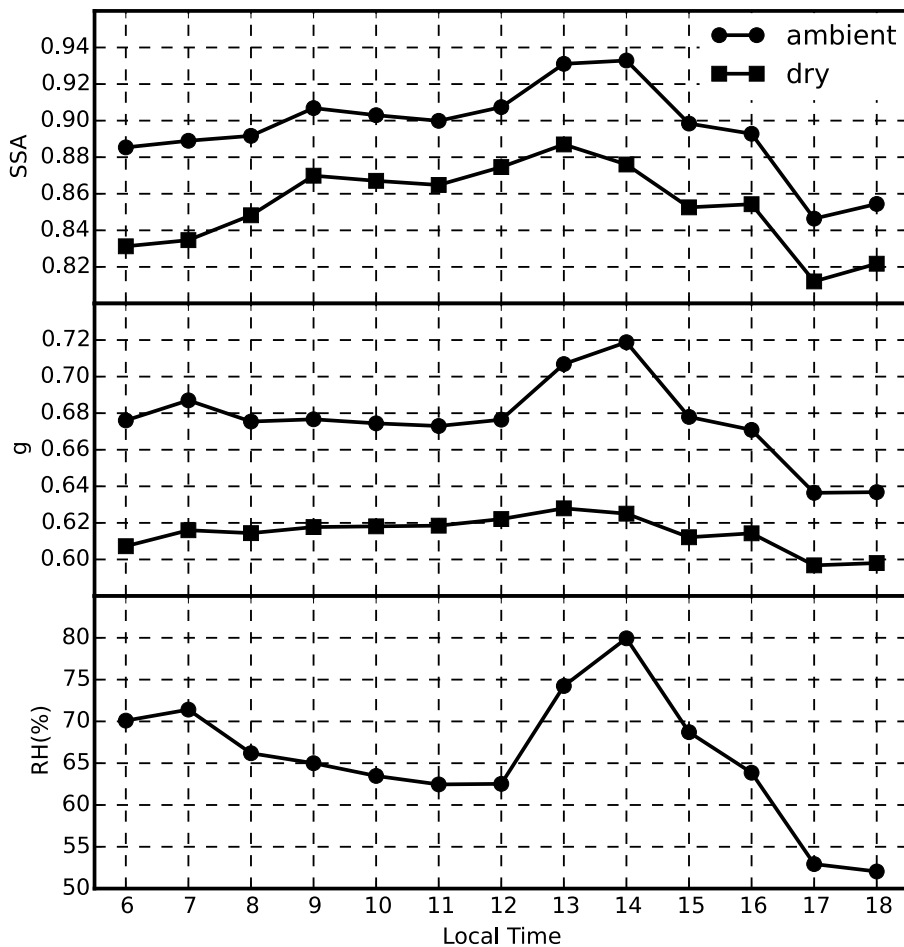
Figure 7. The diurnal variations of SSA, g and RH at the Julian day of 197.